(Received 23 April 2026, Accepted 1 June 2026, Scheduled 25 June 2026)

An Analysis Method for Power Loss of a High-Frequency Transformer with an Interleaved Winding Structure

Rui Zhang[1,*], Honghua Xu[2], and Han Meng[3]

[1]School of Water Conservancy and Hydroelectric Power, Hebei University of Engineering, Handan 056038, China
[2]Institute of Electrical Engineering, Chinese Academy of Sciences, Beijing, China
[3]School of Mining and Geomatics Engineering, Hebei University of Engineering, Handan 056038, China

ABSTRACT: During the switching transient process of high-frequency devices, such as gallium nitride and silicon carbide, an increase in switching frequency will lead to an increase in the distributed leakage inductance (existing between each coil turn and each layer, as well as magnetic flux leakage) and capacitance values (existing between each turn and each layer of each winding, between different windings, and between the winding and the shielding layer). These parasitic parameters will generate sharp voltage peaks, increase power loss, and even cause surge currents and oscillations. To address these issues, this paper proposes an equivalent power-loss model based on a six-layer planar transformer. By designing interleaved coils and introducing variable impedance parameters $X_{1\text{–}2;11\text{–}14;21\text{–}24}$, $d_{1\text{–}2;11\text{–}14;21\text{–}24}$, and $S_{1\text{–}2;11\text{–}14;21\text{–}24}$, this high-frequency transformer can reduce leakage inductance while increasing excitation inductance, thereby significantly reducing the total power loss of the high-frequency transformer. The optimization design of the high-frequency transformer and the analysis of power loss are of great significance for improving the efficiency of high-frequency DC-DC power supply systems.

1. INTRODUCTION

In DC/DC converter systems with a high voltage boost ratio, high-turn-count planar transformers are typically used to achieve high voltage gain. Since the conversion process usually operates in the zero-voltage-switching (ZVS) mode, and the output power is relatively low, the winding losses of the transformer constitute the major portion of the total power loss [1].

The research on multi-winding transformers mainly focuses on the analysis of impedance matrices, the modeling and optimization of optimal current distribution [2].

In terms of loss analysis, optimizing the parallel winding structure of the planar transformer can indirectly optimize its winding losses [3, 4]. In the high-frequency converter system of gapless planar transformers, the magnetic loss generated by the edge leakage flux becomes more dependent on the change of the magnetic core shape as the switching frequency increases [5–7]. High-frequency transformers are also key components that affect the conductive common-mode (CM) electromagnetic interference (EMI) characteristics of switching power supplies [8]. The transformer composed of the matrix structure of the LLC oscillator effectively reduces the leakage inductance and *AC* resistance of the windings, while also significantly reducing the flux offset [9–12]. Therefore, the high-frequency modeling and impedance parameter estimation of high-frequency planar transformers become particularly important [13, 14].

Planar transformers (PTs) have been widely and successfully applied in electric vehicles, new energy power generation, AI data centers, and military systems. However, ensuring the accuracy of the printed circuit board (PCB) design size for planar transformers poses significant challenges [15–17]. Considering the natural leakage inductance value of the transformer, ensuring the ideal width of the primary and secondary coils on both sides of the PCB can reduce copper loss [18, 19]. The segmented arrangement of the planar coil of the transformer, the utilization of coupling inductance, and the integrated current balance control strategy are applicable to the application of power electronic transformers in the high-frequency and high-power domains [20–22]. The height staggered arrangement of the transformer windings, while ensuring the thickness of the copper layer, can eliminate the terminal losses between the PCB boards [23, 24]. Therefore, the PCB analysis model and winding loss calculation for high-frequency and high-power density transformers provide very important theoretical support for the intelligent application prospects of transformers in the future [25].

In summary, in the applications of high-frequency, high-power DC-DC converters and power electronic intelligent artificial intelligence systems with high voltage step-up ratios, as the switching frequency increases, the winding layout, winding losses, impedance parameters, and the design size of the printed circuit board of the high-frequency transformer all require an equivalent power loss model to optimize the configuration of the printed circuit board of the winding. This is to achieve the minimum power loss of the high-frequency planar transformer and provide important theoretical support for the future intelligent application prospects of transformers.

2. ANALYSIS OF THE POWER LOSS MODEL OF THE TRANSFORMER

Currently, planar transformers are the main form of high-frequency electronic transformers. Planar transformers have

* Corresponding author: Rui Zhang (zhangrui@hbgcdx18.wecom.work).

the advantages of being thin and having a large surface area. Since the winding losses and core losses of high-frequency transformers are related to the different structural designs and winding designs of planar transformers, the structural design and winding design of planar transformers must be suitable for the high-frequency working environment. Due to the winding losses caused by the skin effect and proximity effect, the system efficiency and power density are reduced. To reduce the total power loss of magnetic components in high-frequency transformers, it is necessary to lower the peak magnetic flux density of the transformer and the AC resistance value in the winding.

The front view of the planar transformer architecture and structure is shown in Fig. 1. As can be seen from the figure, the 6 layers of coils are located within the transformer core. The middle 2 layers of coils are the primary windings, and the upper and lower 4 layers of coils are the secondary windings.

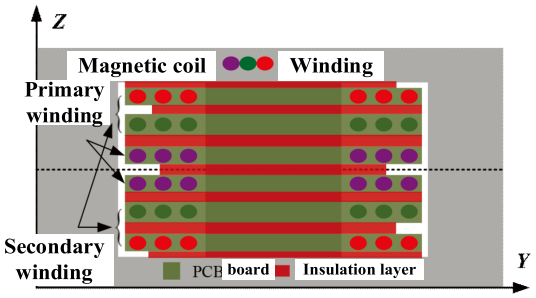

FIGURE 1. Cross-section view of planar transformer structure.

In Fig. 1, based on the front view of the transformer structure, the high-voltage windings on the secondary side are located on the outside, while the low-voltage windings on the primary side are located on the inside. From the top to the bottom of the transformer, they are arranged in the following order: secondary — primary — secondary, alternately placed within the magnetic core. This interleaved arrangement method helps simplify the complexity of the transformer insulation design and reduces the creepage distance and gap distance.

The aforementioned method of interlacing the PCB and windings is shown in Fig. 2. The two half-winding coils are respectively located between the two layers of the PCB. The half-winding coils on the upper and lower layers form a complete winding in space. However, the connections between the pins of different half-winding coils are cross-connections, as shown in Fig. 2. At the cross-connection points, the winding current is reversed, so the direction of the magnetic field generated in

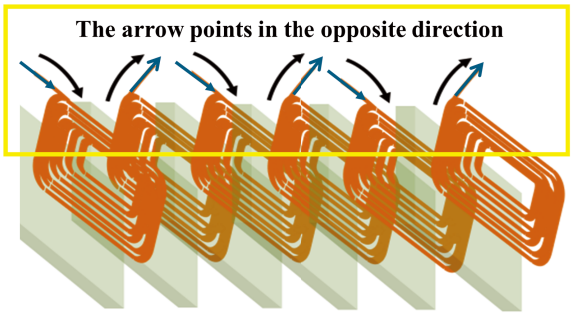

FIGURE 2. PCB and winding layout.

space is also mutually cancelled; that is, all the cross areas are parts of the reduced insulation layer. This not only simplifies the insulation design but also significantly reduces the mixed leakage inductance of the transformer, improving the working efficiency and power density of the transformer. The theoretical correctness of reducing the mixed leakage inductance value can be verified through the transformer equivalent loss model in Fig. 3.

$$\begin{cases} Z_{\text{magnetic\_loss}} = mdSfB_m, \\ Z_{\text{Insulation}} = dSB_mE_m/f, \\ Z_{\text{hybrid}\delta} = dB_mE_m/fS, \\ X_\delta Z_{\text{Insulation}} = X_\delta \cdot dSB_mE_m/f, \\ X_\beta Z_{\text{Insulation}} = X_\beta \cdot dSB_mE_m/f, \\ X_\beta Z'_{\text{Insulation}} = X'_\beta \cdot dSB_mE_m/f, \\ Z_{\text{magnetic\_core}} = mSfB_m/d \end{cases} \tag{1}$$

$$\begin{cases} 11\text{–}14; 21\text{–}24 = \delta, \\ 1\text{–}2 = \beta, \\ X_\delta = \underbrace{\left\{ \pi \left(\sqrt{\left(d_\delta^2 + \left(2\sqrt{\frac{S_\delta}{\pi}} \right)^2 \right)}/2 \right)^2 - S_\delta \right\}}_{A_\delta} \\ \cdot \underbrace{\left\{ \sqrt{\left(d_\delta^2 + \left(2\sqrt{\frac{S_\delta}{\pi}} \right)^2 \right)} - 2\sqrt{\frac{S_\delta}{\pi}} \right\}}_{B_\delta} \\ = A_\delta \cdot B_\delta, \\ X_\beta = A_\beta \cdot B_\beta, \quad X'_\beta = A'_\beta \cdot B'_\beta \end{cases} \tag{2}$$

As shown in Fig. 3, the equivalent model of the six-layer transformer includes a magnetic coil, an insulation layer, a secondary winding, insulation layer, secondary winding, an insulation layer, a primary winding, an insulation layer, a primary winding, an insulation layer, a secondary winding, an insulation layer, a secondary winding, an insulation layer, and a magnetic coil. The six-layer layout consists of 2 layers of primary windings and 4 layers of secondary windings. There is an insulation layer between adjacent layers of the windings, and the outermost layer is the magnetic coil. Each layer of windings of the equivalent transformer is represented in impedance form by the black arrow direction. Eventually, the equivalent model of the planar transformer changes into an impedance circuit equivalent model. The circuit model from left to right is the secondary side — the primary side. In Equation (1), $Z_{\text{magnetic\_loss}}$ represents the impedance related to the magnetic core loss; $Z_{\text{Insulation}}$ represents the impedance related to the area of the insulation layer; $Z_{\text{hybrid}_{11\text{–}14;21\text{–}24}}$ represent the impedances related to the mixed parameters of the primary side and the secondary side; $X_{1\text{–}2;11\text{–}14;21\text{–}24}Z_{\text{Insulation}}$ and $X_{1\text{–}2}Z'_{\text{Insulation}}$ are impedances related to the reduced insulation area, the winding arrangement

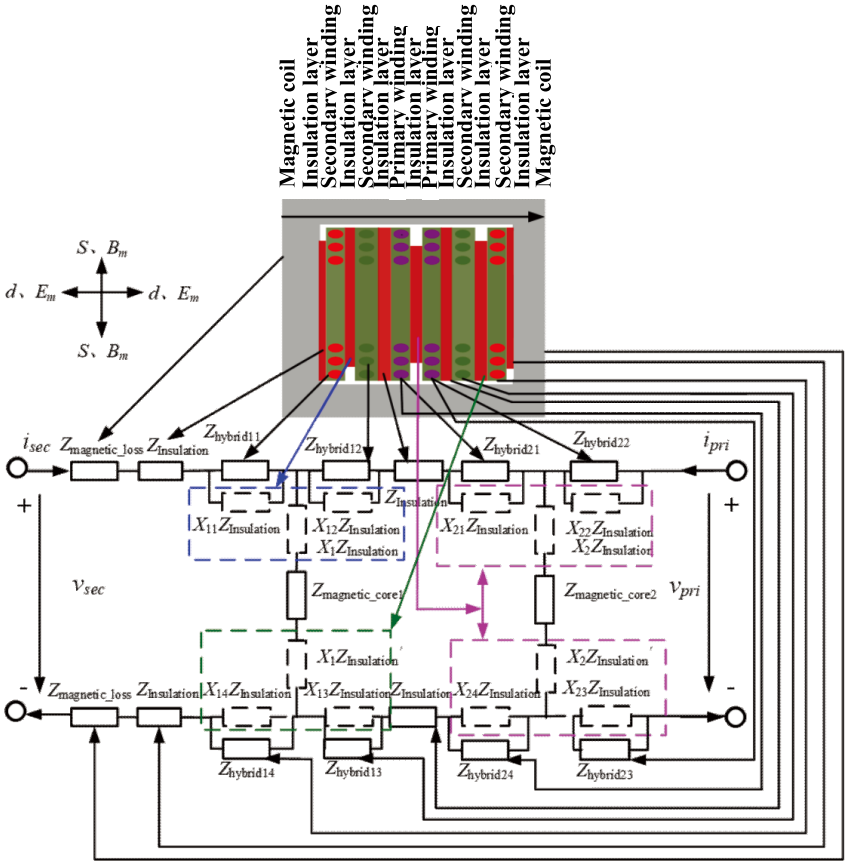

FIGURE 3. Equivalent model of the six-layer transformer.

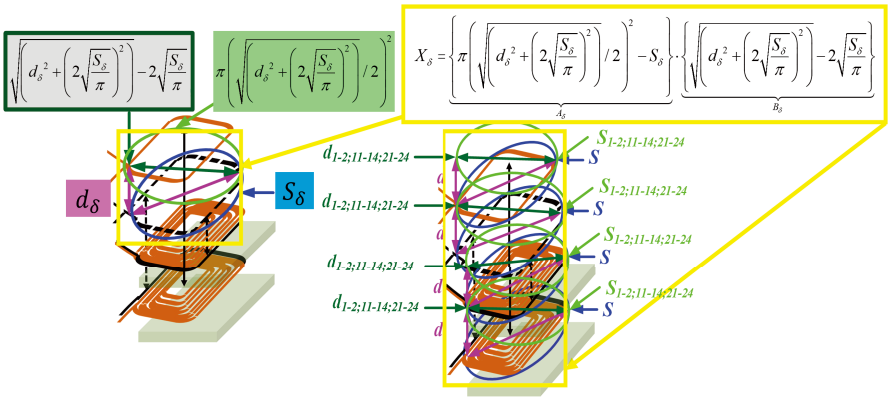

FIGURE 4. X, d, S coefficient relation graph.

between each layer and leakage inductance; $Z_{\text{magnetic\_core}}$ is an impedance related to the power transmitted by the transformer.

As shown in the above equation, $Z_{\text{magnetic\_loss}}$ and $Z_{\text{magnetic\_core}}$ are related to the magnetic field intensity B_m and frequency f of the coil. The horizontal direction variable d in Fig. 3, which is the thickness; the vertical direction variable S in Fig. 3, which is the magnetic flux area and the magnetic core mass m. The impedance with insulating properties is related to the horizontal direction variable d and the electric field intensity E_m, while the vertical direction variable S is related to B_m and f. The difference between Z_{hybrid} and $Z_{\text{Insulation}}$ lies in that Z_{hybrid} is inversely proportional to S, while $Z_{\text{Insulation}}$ is directly proportional to S. $X_{1\text{–}2;11\text{–}14;21\text{–}24}$ are the coefficients related to $d_{1\text{–}2;11\text{–}14;21\text{–}24}$ and $S_{1\text{–}2;11\text{–}14;21\text{–}24}$. These two correlation coefficients are determined by the arrangement pattern between the windings of each layer.

Since each layer of the windings is interconnected with the adjacent layer through its own half-winding, the two half-windings of the upper and lower layers jointly form a complete winding in the space. The position of the complete winding circle changes from the original plane to three-dimensional space. Obviously, compared with the original magnetic flux, the newly formed winding passes through more magnetic flux in space, and the diameter of the approximately circular area

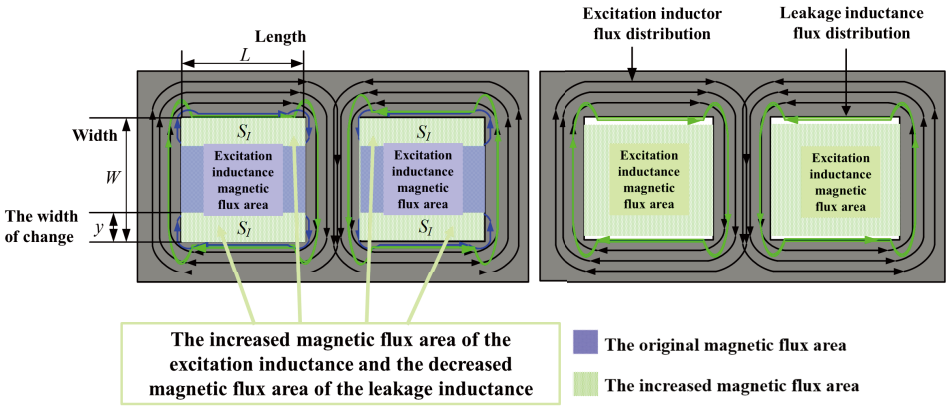

FIGURE 5. The magnetic flux distribution in the planar transformer.

also increases. Due to its position in three-dimensional space, the variables in the horizontal and vertical directions change, and the change amounts are shown in Fig. 3. Therefore, these variables need to be multiplied by coefficients $X_{\beta;\delta}$, which are related to the dimensions of the actual spatial change, $d_{\beta;\delta}$ and $S_{\beta;\delta}$ as shown in Fig. 4.

Regarding the distribution area of magnetic flux in the planar transformer, the specific parameters can be defined as follows.

As can be seen from Fig. 5, the staggered winding arrangement can simultaneously reduce the leakage inductance and increase the excitation inductance, thereby reducing the area of the leakage flux and increasing the area of the excitation flux. The above parameters $X_{\beta;\delta}$, $d_{\beta;\delta}$ and $S_{\beta;\delta}$ can be expressed as:

$$\begin{cases} d_{\beta;\delta} = \sqrt{(W^2 + L^2)}, \\ S_{\beta;\delta} = \pi \dfrac{(W^2 + L^2)}{4}, \\ X_{\beta;\delta} = 4S_I \\ \cdot \left(\sqrt{(W^2 + L^2)} - 2\sqrt{\dfrac{\frac{1}{2}\left(\pi \frac{(W^2+L^2)}{2} - 4S_I\right)}{\pi}} \right) \\ S_I = yL \end{cases} \tag{3}$$

The total power loss of the high-frequency transformer can be calculated as follows [26, 27]:

$$\begin{cases} P_{\text{HF\_T}} = P_{\text{PE}} + P_W + P_C, \\ P_W = I^2 R_{ac}, \\ P_C = \alpha f^c B_{\text{peak}}^d, \\ B_{\text{peak}} = \dfrac{V_{\text{in}}}{4NfA_e}, \\ P_{\text{PE}} = G\dfrac{H^2}{\sigma} \end{cases} \tag{4}$$

$$\begin{cases} R_{ac\_l} = \dfrac{\pi}{4} d\sqrt{f\mu\sigma} R_{dc\_l} \dfrac{\sinh\left(\frac{\pi}{2}d\sqrt{f\mu\sigma}\right) + \sin\left(\frac{\pi}{2}d\sqrt{f\mu\sigma}\right)}{\cosh\left(\frac{\pi}{2}d\sqrt{f\mu\sigma}\right) - \cos\left(\frac{\pi}{2}d\sqrt{f\mu\sigma}\right)} \\ + \dfrac{1}{2}(2l-1)^2 R_{dc\_l} G, \\ R_{dc\_l} = \dfrac{\rho_{cu} L}{\omega t}, \\ G = \dfrac{\pi}{2} d\sqrt{f\mu\sigma} \dfrac{\sinh\left(\frac{\pi}{2}d\sqrt{f\mu\sigma}\right) - \sin\left(\frac{\pi}{2}d\sqrt{f\mu\sigma}\right)}{\cosh\left(\frac{\pi}{2}d\sqrt{f\mu\sigma}\right) + \cos\left(\frac{\pi}{2}d\sqrt{f\mu\sigma}\right)}, \\ \delta = \dfrac{1}{\sqrt{\pi f\mu\sigma}} \end{cases} \tag{5}$$

In formulas (4) and (5), $P_{\text{HF\_T}}$ represents the total power loss of the high-frequency transformer; P_{PE} is the proximity effect loss per unit winding length; P_W is the winding loss of the high-frequency transformer; P_C is the core loss of the high-frequency transformer; A_e is the effective cross-sectional area of the magnetic core; a, c, and d are Steinmetz parameters. The parameter range is: $1 \times 10^{-6} < a < 1.5$, $1 < c < 2$, $1.5 < d < 2$. f is the operating frequency; B_{peak} is the peak magnetic flux density of the N-turn winding with the input voltage of V_{in} of the transformer; $R_{\text{ac},l}$ is the alternating resistance of the l-th layer in the winding; $R_{\text{dc},l}$ is the direct current resistance of the l-th layer in the winding; $\rho_{\text{cu}} = 1.68 \times 10^{-8}\ \Omega/\text{m}$ is the resistivity of copper; μ and σ are the magnetic permeability and electrical conductivity of the copper wire, where $\mu = 4\pi \times 10^{-7}$ H/m; H is the peak external sinusoidal magnetic field caused by the current around the conductor; $\sigma = 58 \times 10^6\ \Omega/\text{m}$, δ is the skin depth.

Therefore, the power loss value of the six-layer planar high-frequency transformer is effectively reduced when the staggered winding arrangement is used compared to the normal arrangement.

As shown in Fig. 6, $Z_{\text{magnetic\_core}}$ increases with the increase of $dX_{\beta;\delta}/dy$, while $Z_{\text{Insulation}}$ and Z_{hybrid} decrease with the increase of $dX_{\beta;\delta}/dy$. The interleaved winding arrangement can reduce the leakage inductance while increasing the excitation inductance. Due to the increase in the magnetic flux area $S_{\beta;\delta}$ of the excitation inductance, the peak magnetic flux density of the transformer will decrease. The reduction of $Z_{\text{Insulation}}$ and Z_{hybrid} leads to a decrease in the AC resistance value of the

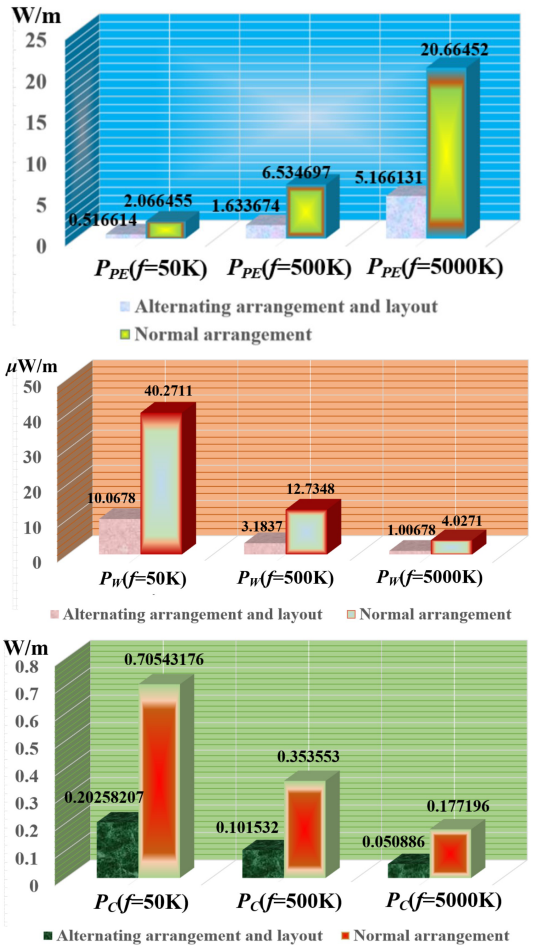

FIGURE 6. Loss comparison between alternating arrangement and normal arrangement.

windings. As $dX_{\beta;\delta}/dy$ increases, the proximity effect loss P_{PE} per unit winding length, the winding loss P_W of the high-frequency transformer, and the core loss P_C will decrease.

3. CONCLUSION

With variations in frequency, the number of turns per winding, and the number of layers, the leakage inductance, excitation inductance, and mixed impedance values of the interleaved winding are smaller than those of the traditional complete winding arrangement method. Moreover, the changes in the excitation inductance and mixed impedance values of the interleaved winding are very small. Clearly, as the number of layers increases and the number of turns decreases, the leakage inductance can be significantly reduced. The influence of increasing the number of layers is more obvious than that of decreasing the number of turns, making it more suitable for the application of the interleaved winding arrangement method. As the number of layers increases, the leakage inductance decreases; the excitation inductance increases; and the mixed impedance remains constant. The interleaved winding arrangement can reduce the leakage inductance and simultaneously increase the excitation inductance.

ACKNOWLEDGEMENT

This paper is supported by the Natural Science Foundation Project of Hebei Province E2024402072, E2025402096, and Scientific Research (Youth Top) Project of the Higher Education Department of Hebei Province BJ2025031.

REFERENCES

[1] Lin, J., Y. Yang, S. Yin, X. Xin, R. Wang, M. Dong, and H. Li, "Loss model of high-frequency planar transformer for high-voltage resonant DC/DC converter," in *2020 IEEE Workshop on Wide Bandgap Power Devices and Applications in Asia (WiPDA Asia)*, 1–7, Suita, Japan, 2020.

[2] Datta, K., Y. Wu, C. R. Sullivan, and J. T. Stauth, "Optimal current distribution in multi-winding transformers for isolated and wireless power transfer," *IEEE Open Journal of Power Electronics*, Vol. 6, 1296–1309, 2025.

[3] He, M., J. Xie, L. Yang, W. Chen, S. Lin, Q. Chen, and Y. Huang, "Analysis of connection optimization in planar transformer winding loss," in *2023 IEEE 2nd International Power Electronics and Application Symposium (PEAS)*, 604–607, Guangzhou, China, 2023.

[4] Qian, Z., Q. Chen, B. Xie, W. Chen, Y. Lan, and L. Ru, "Two-dimensional winding loss modeling of planar inductors considering the effect of air-gap diffusion flux," in *2024 2nd China Power Supply Society Electromagnetic Compatibility Conference (CPEMC)*, 53–58, Hangzhou, China, 2024.

[5] Shafaei, R., M. C. G. Perez, and M. Ordonez, "Planar transformers in LLC resonant converters: High-frequency fringing losses modeling," *IEEE Transactions on Power Electronics*, Vol. 35, No. 9, 9632–9649, Sep. 2020.

[6] Yoo, J. and J. Kim, "Comparison and analysis of high frequency planar transformer characteristic for DC-DC converter," in *2021 24th International Conference on Electrical Machines and Systems (ICEMS)*, 2074–2078, Gyeongju, Korea, 2021.

[7] Bouvier, Y. E., G. Salinas, A. Stanojević, and P. J. Grbović, "Optimization of custom ferrite e-core-shaped transformers for power loss and volume reduction using pareto front analysis," in *2023 22nd International Symposium on Power Electronics (Ee)*, 1–6, Novi Sad, Serbia, 2023.

[8] Hou, L., S. Lin, and C. Peng, "Study on common mode EMI characteristic modeling method of planar transformer," in *2023 IEEE 2nd International Power Electronics and Application Symposium (PEAS)*, 1826–1830, Guangzhou, China, 2023.

[9] Zhang, H., Y. Guan, Y. Wang, and D. Xu, "A high-frequency LLC resonant converter incorporating matrix transformer," in *2025 IEEE Workshop on Wide Bandgap Power Devices and Applications in Asia (WiPDA Asia)*, 1–6, Beijing, China, 2025.

[10] Zheng, Y., Y. Wu, S. Wang, and Z. Shen, "Optimal design of the planar transformer based on its multi-physics field coupling characteristics," in *2023 IEEE 14th International Symposium on Power Electronics for Distributed Generation Systems (PEDG)*, 786–791, Shanghai, China, 2023.

[11] Da Silva, J. L., I. B. Pinheiro, P. H. C. Lopes, G. M. Soares, and P. S. Almeida, "An lti transformer model via admittance formulation and hybrid parameter extraction for parasitic-aware analysis of high-frequency isolated power converters," *IEEE Access*, Vol. 13, 181 016–181 028, 2025.

[12] Jang, J. and Y. Cho, "Design of an integrated planar magnetic-based LLC resonant converter for enhanced power density in aircraft power systems," in *2025 28th International Conference on Electrical Machines and Systems (ICEMS)*, 2924–2928, Busan,

Korea, 2025.

[13] Rasmann, R., V. Golev, U. Schumann, and J. Schnack, "Automated design and optimization of planar transformers for high-frequency applications," in *2023 IEEE Design Methodologies Conference (DMC)*, 1–6, Miami, FL, USA, 2023.

[14] Ahmed, D., L. Wang, M. Wu, L. Mao, and X. Wang, "Two-dimensional winding loss analytical model for high-frequency multilayer air-core planar inductor," *IEEE Transactions on Industrial Electronics*, Vol. 69, No. 7, 6794–6804, Jul. 2022.

[15] Gaikwad, C. B., V. S. Rajguru, and S. P. Adhau, "Performance analysis of planar transformer for DC-DC converter with ansys maxwell," in *2022 International Conference on Emerging Trends in Engineering and Medical Sciences (ICETEMS)*, 247–251, Nagpur, India, 2022.

[16] Jamshed, F., R. Mounesi, and A. Nasiri, "Fem-based design and experimental validation of a high power density planar transformer for an active clamp flyback converter," in *2025 14th International Conference on Renewable Energy Research and Applications (ICRERA)*, 1159–1163, Vienna, Austria, 2025.

[17] Hassan, M. I., N. Keshmiri, A. D. Callegaro, M. F. Cruz, M. Narimani, and A. Emadi, "Design optimization methodology for planar transformers for more electric aircraft," *IEEE Open Journal of The Industrial Electronics Society*, Vol. 2, 568–583, 2021.

[18] Kim, M. and E. S. Lee, "Optimal design of planar transformer for DAB converters based on model-free reinforcement learning," in *2025 IEEE Energy Conversion Congress & Exposition Asia (ECCE-Asia)*, 1–5, Bengaluru, India, 2025.

[19] McLean, J. S., "Guanella transformer/balun implemented with planar transformer technology," in *2022 IEEE Texas Symposium on Wireless and Microwave Circuits and Systems (WMCS)*, 1–6, Waco, TX, USA, 2022.

[20] Kong, D., Q. Min, S. Lu, and S. Li, "A high-frequency high-power transformer based on split planar coils for high-isolation applications," in *2021 IEEE 4th International Electrical and Energy Conference (CIEEC)*, 1–5, Wuhan, China, 2021.

[21] Dou, Y., Z. Ouyang, and M. A. E. Andersen, "Design the high-frequency DC-DC converter with integrated coupled inductor and current-balancing-transformer," in *2020 IEEE Applied Power Electronics Conference and Exposition (APEC)*, 2610–2616, New Orleans, LA, USA, 2020.

[22] Wouters, H., X. Shen, H. Pervaiz, and W. Martinez, "Optimisation of magnetic loss trade-offs in high-frequency litz wire transformers," in *2023 25th European Conference on Power Electronics and Applications (EPE'23 ECCE Europe)*, 1–11, Aalborg, Denmark, 2023.

[23] Soundararajan, S. G., H. Wouters, W. Vanderwegen, and W. Martinez, "Folded flex-PCB winding planar transformer for high-frequency isolated DC-DC converters," in *2025 IEEE Applied Power Electronics Conference and Exposition (APEC)*, 238–245, Atlanta, GA, USA, 2025.

[24] Liang, Y., Y.-H. Hsieh, and Q. Li, "Equivalent circuit-based analysis of current sharing in planar transformer parallel windings," in *2025 IEEE Energy Conversion Conference Congress and Exposition (ECCE)*, 1–8, Philadelphia, PA, USA, 2025.

[25] Kwon, H., J. Lee, J. Lee, and J.-I. Ha, "Analytical modeling and design of 27.12 MHz single-switch DC–DC converter with PCB transformer," *IEEE Access*, Vol. 11, 12 742–12 754, 2023.